Cellular and Molecular Life Sciences (2024) 81:366
https://doi.org/10.1007/s00018-024-05413-x

ORIGINAL ARTICLE

RetSat stabilizes mitotic chromosome segregation in pluripotent stem cells

Wanzhi Cai[1,3] · Xiaoqing Yao[1,3] · Gaojing Liu[2,3] · Xiuyun Liu[2,3] · Bo Zhao[2] · Peng Shi[1,4]

Received: 27 March 2024 / Revised: 4 July 2024 / Accepted: 16 August 2024

Abstract

Background Chromosome stability is crucial for homeostasis of pluripotent stem cells (PSCs) and early-stage embryonic development. Chromosomal defects may raise carcinogenic risks in regenerative medicine when using PSCs as original materials. However, the detailed mechanism regarding PSCs chromosome stability maintenance is not fully understood.

Methods Mouse embryonic stem cells (line D3) and human embryonic stem cells (line H9) were cultured under standard conditions. To confirm the loading of RetSat protein on mitotic chromosomes of PSCs, immunostaining was performed in PSCs spontaneous differentiation assay and iPSC reprogramming assay from mouse embryonic fibroblasts (MEFs), respectively. In addition, qPCR, immunoprecipitation, LC-MS/MS and immunoblotting were used to study the expression of RetSat, and interactions of RetSat with cohesin/condensin components. RNA sequencing and teratoma formation assay was conducted to evaluate the carcinogenic risk of mouse embryonic stem cells with RetSat deletion.

Results We reported a PSC high-expressing gene, *RetSat*, plays key roles in chromosome stabilization. We identified RetSat protein localizing onto mitotic chromosomes specifically in stemness positive cells such as embryonic stem cells (ESCs) and induced pluripotent stem cells (iPSCs). We found dramatic chromosome instability, e.g. chromosome bridging, lagging and interphase micronuclei in mouse and human ESCs when down regulating *RetSat*. *RetSat* knock-out mouse ESCs upregulated cancer associated gene pathways, and displayed higher tumorigenic capacities in teratoma formation assay. Mechanistically, we confirmed that RetSat interacts with cohesin/condensin components Smc1a and Nudcd2. RetSat deletion impaired the chromosome loading dosage of Smc1a, Smc3 and Nudcd2.

Conclusions In summary, we reported RetSat to be a key stabilizer of chromosome condensation in pluripotent stem cells. This highlights the crucial roles of RetSat in early-stage embryonic development, and potential value of RetSat as an effective biomarker for assessing the quality of pluripotent stem cells.

Keywords Retinol saturase · Chromosome loading · Chromosome mis-segregation · Carcinogenesis

Introduction

Chromosome stability is crucial for early embryonic development. Existing studies support the notion that both numerical and structural instability of chromosome instability (CIN) impair the embryonic developmental process. For example, approximately 70% human early-stage embryos exhibit aneuploidy, which may lead to abnormal embryonic development or lethality [1]. Micronuclei are a typical representation of structural CIN. Micronuclei can result in reduced developmental potential in early embryos, particularly affecting the pregnancy rate after embryo transplantation in assisted reproduction [2]. Pluripotent stem cells (PSCs) including embryonic stem cells (ESCs) and induced pluripotent stem cells (iPSCs) are used as in vitro tools in

Wanzhi Cai and Xiaoqing Yao contributed equally to this work.

✉ Bo Zhao
zhaobo@mail.kiz.ac.cn

✉ Peng Shi
ship@mail.kiz.ac.cn

1 Key Laboratory of Genetic Evolution & Animal Models, Kunming Institute of Zoology, Chinese Academy of Sciences, Kunming, Yunnan 650223, China

2 Key Laboratory of Animal Models and Human Disease Mechanisms, Kunming Institute of Zoology, Chinese Academy of Sciences, Kunming, China

3 University of Chinese Academy of Sciences, Beijing, China

4 School of Future Technology, University of Chinese Academy of Sciences, Beijing 101408, China

Published online: 22 August 2024

current developmental biology research and investigations into the mechanisms of developmental diseases broadly [3, 4]. Additionally, high-quality embryonic stem cells and induced pluripotent stem cells serve as fundamental components in regenerative medicine applications. However, in the current in vitro culture and expansion processes of pluripotent stem cells, challenges related to CIN are encountered. CIN weakens the stemness of pluripotent stem cells and increases carcinogenesis risks [5]. Therefore, in-depth research on CIN in pluripotent stem cells is of great significance, both for fundamental research on embryonic development and for applications in assisted reproduction and regenerative medicine.

PSCs exhibit unique characters in chromosome stabilization and genomic stabilization compared to differentiated counterparts. To achieve dynamic changes in chromatin landscape to express diverse genes and global chromosome condensation upon lineage differentiation, PSCs need meiosis-specific REC8-STAG3 cohesin complex in mitotic ESCs to safeguard chromosome stability [6]. In addition, PSCs hold high expression of DNA damage response genes, meanwhile express unique genes *Filia*, *Floped*, *Zscan4*, *Dcaf11* and long non-coding RNAs *Discn*, *Lnc956* and *Lnc530* to enhance homologous recombination mediated double-strand break DNA repair [7, 8], stalled fork restarting [9, 10], telomeric protection [11, 12], RPA availability and DNA metabolism [13]. Consequently, either down-regulation of these unique genes or dysfunction of cohesin/condensin complexes impairs self-renewal capacities and stemness, which links to carcinogenic risks in stem cell translational usage, or human embryonic failure at early developmental stage [14].

RetSat (official name: Retinol Saturase) encoded protein has both cytoplasmic and nuclear localization [15, 16]. In cytoplasm, it plays roles as an oxidoreductase in endoplasmic reticulum (ER) to transforms retinol into 13,14-dihydroretinol predominantly. Some transcriptional factors such as PPARα in liver [17], PPARγ in adipose tissue [18] and FOXO1 in primary hepatocytes [19] were reported to be upstream regulators of RetSat. We reported that *RetSat* is a convergent gene in mammalian adaptation to hypoxia on the Qinghai-Tibetan Plateau, and the amino acid switch from glutamine (Q) to arginine (R) at the position 247 (Q247R) of RetSat is responsible for heart function enhancement and mammalian adaptation to hypoxia [20]. We also found that nuclear RetSat associates with RNA helicase DDX39B to promote stalled fork restarting under gemcitabine induced replicative stress, which finally impart cellular tolerance to severe hypoxia in pancreatic ductal adenocarcinoma research models [21]. Indeed, other studies also reported that knocking down RetSat protects fibroblasts from ultra violet (UV) or paraquat induced oxidative stress [22], further supporting the notion that RetSat is functional in oxidative homeostasis, or even UV induced DNA damage response and genomic stability. However, the functions of RetSat in mitotic chromosome stability are still misty.

RetSat displayed active viewpoints similar to pluripotent factor Nanog in embryonic stem cells when study the genome topological dynamics using 4C (chromosome conformation capture combined with sequencing) technologies [23]. This reminds the possibility that RetSat plays roles matching ESCs unique chromosome stabilization. In this study, we reported RetSat as a chromosome binding protein specifically in stemness positive cells. RetSat promotes loading of Smc1a, Smc3 and Nudcd2 on anaphase chromosomes, key components for chromosome stabilization. RetSat deletion caused chromosome mis-segregation in mitotic mESC, such as chromosomal bridge, lagging and micronuclei. We also found that RetSat loss lead to oncogenic transformation of mESC, highlighting the potential value of RetSat in quality control of PSCs. In summary, we defined RetSat to be a PSC specific chromosome stabilizer.

Materials and methods

Animals

All mice were housed in an authorized animal facility at Kunming Institute of Zoology, Chinese Academy of Sciences (CAS). Mice were housed in individually ventilated cages using a 12-hour light/12-hour dark cycle. All animal experiments used in this study were conducted according to the guidelines approved by the Ethics Committee of Kunming Animal Research Institute. Approval No: SMKX-20200710-37.

Generation of *RetSat*-knockout mice

Construction of gene editing mice was performed by Cyagen Biosciences, Inc. Briefly, exons 2–11 of *RetSat* gene were selected to be target site covering 6406 base pair. Cas9 endonuclease and 4 sgRNAs were co-injected into fertilized eggs and transplanted into the recipient female mouse. Two heterozygous females and two heterozygous males were born in generation P0. The pups were genotyped by PCR and sequencing analysis. Two pairs of primers were designed for identifying of genotype, the sequence of primer 1 (5'-3', F: GCTTCTTCCAAAGAAACCCAGTTC, R: CTGAAAGA ATTCTGACTCCAAGCA, product size: 483 bp), primer 2 (5'-3', F: CTTATTGCCTTTTCTTTCCTCGCTT, R: AAG CCTTACCAGTGTCAAATTCAAG, product size: 682 bp). Mouse genomic DNA was extracted by standard method using DNA extraction kit (TIANGEN, Cat. no. DP304).

1 μg DNA was used as the amplification template for PCR experiment, and the PCR reaction was performed by Premix Ex Taq (Takara, Cat. no. RR902A) in a 25 μL reaction system. Reaction condition was initial denaturation at 94 °C for 3 min, denaturation at 94 °C for 30 s, annealing at 60 °C for 35 s, extension at 72 °C for 35 s and 35 cycles from second step, finally additional extension at 72 °C for 5 min. DNA bands were detected by 1.5% agarose gel electrophoresis. Homozygotes showed one band of 483 bp, wildtype allele showed one band with 682 bp and heterozygotes showed two bands both (Supplementary Fig. 1c).

Derivation of stem cell lines from *RetSat* wild-type/knock-out mouse embryos

mESCs were isolated from *RetSat* wild-type/knock-out mice followed by standard operating procedures [24]. In brief, administer 5 IU PMSG (Acmec, Cat. no. AP9970) injection to 4–6 weeks old nulliparous female mice from the C57BL/6J strain, after 48 h, administer 5 IU HCG (Acmec, Cat. no. C79010) injection, and mate the females with 8–10 weeks old male mouse at 1:1 ratio. After checking the copulatory plugs, the females were separated from the males next day. The female mice were euthanized by cervical dislocation 45–48 h post-coitum. The oviducts were cut off after dissection, followed by flush with Hepes-buffered CZB medium (HCZB) and 2-cell embryos were collected. The embryos were picked up using the mouth pipette apparatus into the KSOM medium and cultured embryos until to the blastocyst stage at 37 °C under 5% CO_2 culture conditions. The zona pellucida of embryos were removed using acidic Tyrode's solution followed by seeding one zona-free blastocyst on the feeder cells in each plate well. Monitoring the outgrowth formation, change half of 2i + LIF culture medium every other day. The outgrowth was digested into pieces after 6–8 days culture in order to release the ICM cells and further expansion.

Cell lines and culture

Mouse embryonic fibroblasts (MEF) were isolated from C57BL/6J mouse embryos at Embryonic day 13.5 (E13.5). Human somatic fibroblasts (HEL-1) were purchased from the Conservation Genetics CAS Kunming Cell Bank (China). Mouse embryonic stem cells (mESCs, line D3) and human embryonic stem cells (hESCs, line H9) were kindly provided by Professor Ping Zheng laboratory at Kunming Institute of Zoology, CAS. HEK293 cells were purchased from ATCC (Cat. no. CRL-1573).

MEF, HEL-1, and HEK293T cells were cultured in DMEM medium (Gibco, Cat. no. C11995500BT) consisting of 10% FBS (Gibco, Cat. no. 16000-044) and 1% penicillin/streptomycin supplement (Gibco, Cat. no. 15140122). The mouse induced pluripotent stem cells (miPSCs) were reprogrammed from ICR mouse embryonic fibroblasts (MEF) by transduction of retroviral vectors encoding Oct-4/Sox2/Klf4/c-Myc transcription factors, OSKM were kindly donated from Professor Zheng Ping's laboratory at Kunming Institute of Zoology, CAS. miPSCs were cultured on feeder with 2i/LIF medium. hESCs were cultured in Human Pluripotent Stem Cell Medium (Cauliscel, Cat. no. 400105). mESCs were cultured on plates coated with 0.1% gelatin (Amersco, Cat. no. 9764) in culture media containing Dulbecco's Modified Eagle's Medium (DMEM) (Gibco, Cat. no. C11995500BT) supplemented with 15% FBS (Gibco, Cat. no. 16000-044), 2 mM Gluta MAX Supplement (Gibco, Cat. no. 35050061), 100 U/mL penicillin and 100 μg/mL streptomycin (Gibco, Cat. no. 15140122), 0.1 mM β-mercaptoethanol (Gibco, Cat. no. 21985023), 0.1 mM nonessential amino acids (Gibco, Cat. no. 11140-035), 1 mM sodium pyruvate (Gibco, Cat. no. 11360070), supplemented with two small molecular inhibitors 1 μM PD0325901 (Selleck, Cat. no. S1036), 3 μM CHIR99021 (Selleck, Cat. no. S1263) and 1000 U/mL LIF (Millipore, Cat. no. ESG1106).

Differentiation assay of mESCs

For the mESCs differentiation assay, feeder was replaced with 0.1% gelatin. For spontaneous differentiation, mESCs were cultured in LIF-free medium for 15 days. For all-trans retinoic acid induced neuroectodermal and extraembryonic endoderm differentiation, mESCs were cultured in LIF-free medium supplemented with 250 nM all-trans retinoic acid (Sigma, Cat. no. 554720) for 48 h. After treatment, fresh media were changed every two days, cells were harvested at day 15 for gene expression analysis and immunostaining.

Lentivirus mediated RetSat gene expression

Mouse *RetSat* coding region was constructed into pTOMO-IRES-EGFP vector (Addgene plasmid.

#26291) through BamHI and XbaI digest sites. The lentiviral vectors were transfected into HEK293T.

cells along with the packaging plasmids psPAX2 and pMD2.G at a ratio of 5:2.5:1 using Lipofectamine 3000.

(Invitrogen, Cat. no. L3000015). Lentivirus was harvested 48 h post transfection and fltered with 0.45 μm flter (Millipore, Cat. no. SLHV033RB). *RetSat* knockout mESCs were infected with lentivirus and screened with 3 μg/mL puromycin 72 h post infection [25].

Chemicals and antibodies

Aphidicolin was purchased from Sigma-Aldrich (Cat. No. 38966-21-1; 1MG). Reversine was purchased from Sigma-Aldrich (Cat. No. 656820-32-5; 1MG). The following antibodies were obtained from the indicated suppliers: rabbit anti-RetSat polyclonal antibody (Invitrogen, Cat. No. PA5-65443, 1:1000 for immunoblotting), mouse anti-RetSat monoclonal antibody (made in our laboratory, we have isolated and purified a high concentration of single epitope specific RetSat monoclonal antibody at a concentration of ~0.8 mg/ml after fusion culture and screening of hybridoma cells from mice immunized with RetSat antigen, 1:400 for immunoblotting, 1:20 for immunofluorescence and 3 µg for immunoprecipitation), rabbit anti-Aurora B polyclonal antibody (Abcam, Cat. No. ab2254, 1:500 for immunofluorescence), rabbit anti-Oct4 monoclonal antibody (Abcam, Cat. No. ab181557, 1:1000 for immunoblotting), rabbit anti-Sox2 monoclonal antibody (Abcam, Cat. No. ab92494, 1:1000 for immunoblotting), rabbit anti-Nudcd2 polyclonal antibody (Proteintech, Cat. No. 21205-1-AP, 1:1000 for immunoblotting), mouse anti-Smc1a monoclonal antibody (Proteintech, Cat. No. 66987-1-Ig, 1:1000 for immunoblotting), rabbit anti-Smc3 polyclonal antibody (Proteintech, Cat. No. 14185-1-AP, 1:500 for immunoblotting), mouse anti-Gapdh monoclonal antibody (Beyotime, Cat. No. AF0006, 1:1000 for immunoblotting), mouse anti-β-Actin monoclonal antibody (Sigma-Aldrich, Cat. No. A1978, 1:2000 for immunoblotting), rabbit anti-Histone H2A polyclonal antibody (Beyotime, Cat. No. AH419, 1:1000 for immunoblotting), mouse IgG antibody (Beyotime, Cat. No. A7028, 1 µg for immunoprecipitation). The secondary antibodies used were raised against mouse conjugated with Alexa Flour 594 (ThermoFisher, Cat. no. A-11005, 1:500 for immunofluorescence), against rabbit conjugated with Alexa Flour 488 (ThermoFisher, Cat. no. A-11008, 1:500 for immunofluorescence), goat anti-mouse IgG antibody conjugated with HRP (Sigma-Aldrich, Cat. no. A4416, 1:2000 for immunoblotting), goat anti-rabbit IgG antibody conjugated with HRP (Sigma-Aldrich, Cat. no. A0545, 1:3000 for immunoblotting).

Immunoblotting

Cells were gently washed with ice-cold PBS and collected by cell scraping. The cells were lysed on ice for 30 min with RIPA lysis buffer (150 mM NaCl, 1% Triton X-100, 0.1% SDS, 50 mM Tris Base, 1 mM EDTA in ddH_2O, PH = 7.4) containing of 1X proteinase inhibitor cocktail (BIMAKE, Cat. no. B14001) after centrifugation, then sonication was performed at 30 HZ for 5 min (Sonics, Cat. no. VCX130/130 PB). Protein concentration was quantified by Bradford method (Beyotime, Cat. No. P0006). Equal amount of protein was separated on SDS-PAGE gels using running buffer and transfer to 0.45 µm PVDF membranes (Millipore, Cat. no. IPVH00010) at 300 mA for 90 min in ice-cold transfer buffer. Membranes were blocked with 5% skim milk (Oxoid, Cat. no. LP0033B) in PBST at room temperature for 1 h, incubated with primary antibody at 4 °C overnight, washed with TBST 3 times for 5 min each time, followed by incubation with HRP-conjugated secondary antibodies diluted with TBST containing 3% skim milk at room temperature for 1 h, finally washed with TBST for 3 times and blots were developed using Immobilon Forte Western HRP substrate (Millipore, Cat. no. WBKLS0500) with Luminescence Imaging System (Tanon 5200).

Immunofluorescence

Coverslips of 24-well plate (NEST, Cat. no. 801007) were coated with Matrigel (BD Biocoat, Cat. no. 354277) diluted 1:10 in culture medium for mESC/miPSC/hESC cells, or coated with 100 µg/mL Poly-L-Lysine (Sigma-Aldrich, Cat. no. P1399) for MEF/HEL-1/HEK293T cells. The cells were seeded onto coverslips in 24-well plate before fixed with 4% paraformaldehyde (Sigma-Aldrich, Cat. no. P6148) at room temperature for 1 h. Then cells were washed with PBST and permeabilized with 0.3% Triton X 100 solution (Sigma-Aldrich, Cat. no. T8787) for 15 min at room temperature. Cells were blocked with 5% bovine serum albumin (Sigma-Aldrich, Cat. no. A1933) in PBS for 1 h at room temperature, followed by incubation with primary antibody at 4 °C overnight, washed with PBST for 3 times and incubated with secondary antibody 1 h at room temperature. After washed with PBST 3 times, the coverslips were inverted onto a drop of anti-fading mounting medium (Solarbio, Cat. no. S2110 containing DAPI). Images were taken using Olympus FV1000 confocal microscopes under 100X lens.

Real-time RT-PCR

The cells were centrifugally collected after digestion with trypsin. Tissues were ground into homogenates by freezing grinder (LUKYM, Guang Zhou, China) followed by lysed with QIAzol Lysis Reagent (QIAGEN, Cat. no. 79306). Total RNA was extracted using RNeasy Mini Kit (QIAGEN, Cat. no. 74104) and determined concentration by Nanodrop 2000. First-strand complementary DNA was synthesized by PrimeScript RT reagent Kit (Takara, Cat. no. RR037Q). qPCR was performed by standard protocol using GoTaq qPCR Master Mix (Promega, Cat. no. A6001). The primers sequences used for quantitative RT-PCR are as follows: mouse *RetSat* (forward: 5'-GCACTTGTTGCCAGA

GACTGTC-3', reverse: 5'-TTCAGGTCCTCCTTGGTGC CTT-3'); mouse *Oct4* (forward: 5'-CGGAAGAGAAAGC GAACTAGC-3', reverse: 5'-ATTGGCGATGTGAGTGAT CTG-3'); mouse *Sox2* (forward: 5'-GCGGAGTGGAAAC TTTTGTCC-3', reverse: 5'-GGGAAGCGTGTACTTATC CTTCT-3'); mouse *Nanog* (forward: 5'-CACAGTTTGCC TAGTTCTGAGG-3', reverse: 5'-GCAAGAATAGTTCTC GGGATGAA-3') ; mouse *Gapdh* (forward: 5'-TGACCTC AACTACATGGTCTACA-3', reverse: 5'-CTTCCCATTCT CGGCCTTG-3'). Gene expression was quantified relative to housekeeping gene *Gapdh* as an internal control based on the threshold cycle (Ct) at fluorescence intensity. Relative expression of target gene was calculated using formula $2^{-(\Delta Ct(sample)-\Delta Ct(control))}$.

Immunohistochemistry

Formalin-fixed paraffin embedded tissue Sect. (4 μm) were deparaffinized and hydrated by incubating sections in three washes of environmental dewaxing dip wax transparentize solution (Servicebio, Cat. no. G1128-1 L) for 15 min each, followed by two washes of 100% ethanol for 10 min each, two washes of 95% ethanol for 5 min each, 90% ethanol for 3 min, 80% ethanol for 2 min, 70% ethanol 1 min and three washes of ddH_2O for 5 min each. Antigens were retrieved by boiling slides in citrate antigen retrieval solution (Beyotime, Cat. no. P0081), maintained at a sub-boiling temperature for 8 min and cooled to room temperature. Hematoxylin and eosin (HE) staining was conducted following standard procedures. Briefly, tissue sections were stained with hematoxylin solution (Servicebio, Cat. no. G1004) for 3 min followed by water rinse for 1 min. Then the sections were treated with 1% hydrochloric acid solution for 15 s, quickly processed sections in 1% ammonium hydroxide for 15 s, followed gentle rinse of water for 1 min. Then the sections were stained with eosin solution (Servicebio, Cat. no. G1005) for 3 min and followed by dehydration with graded alcohol and clearing in xylene. Seal the slides with neutral resin and dry the resin at room temperature.

Immunoprecipitation

The mESCs were treated with 0.05 μg/ml nocodazole (Solarbio, Cat. no. IN0710) for 6 h at 37 °C under 5% CO_2 culture conditions, which synchronized cells to G2/M phase. After remove nocodazole, cells were lysed with RIPA buffer, cell precipitates collected from each 150 mm^2 dishes add 1 mL RIPA lysis buffer. For immunoprecipitation (IP) assay, 25 μL protein A/G agarose beads (YEASEN, Cat. no. 36403ES03) were pre-washed three times with RIPA, centrifuged at 4500 rpm for 2 minutes and supernatant was removed, then incubated cell lysates with the beads in the absence of an antibody to control for non-specific binding, under the condition at 4 °C on 4-dimensional rotator for 3 h. After 4500 rpm centrifugation for 2 minutes and gently suck out supernatant, add 3 μg RetSat primary antibody and incubated at 4 °C on 4-dimensional rotator for 17 h, 1 μg mouse IgG antibody (Beyotime, Cat. no. A7028) was added another as negative control. Followed by pre-washed of RIPA buffer, 60 μL protein A + G beads were added into supernatant from previous step, incubated antibody-conjugated beads at 4 °C on 4-dimensional rotator for 5 h. The supernatant was centrifugally sucked out and precipitated beads were washed with RIPA for 6 times, the last three times change wash buffer to hyperhaline RIPA (300 mM NaCl, 1% Triton X-100, 0.1% SDS, 50 mM Tris Base, 1 mM EDTA in ddH_2O, pH = 7.4), the beads were wash on 4-dimensional rotator for 7 min each time, and re-suspended the beads in 50 μL 2X SDS loading buffer (Beyotime, Cat. no. P0015) and eluted protein complexes from beads by boiling for 10 min, balanced to room temperature, centrifuge at 15,000 rpm for 5 min then subjected to immunoblotting analysis. The SDS-PAGE gel of major protein was stained with silver performed by standard procedures using the Silver Stain Kit (Beyotime, Cat. no. P0017S). The mass spectrum analysis was conducted by Novogene Company.

RNA-seq analysis

For mESCs RNA-seq analysis, total RNA was extracted by RNeasy Mini Kit (QIAGEN, Cat. no. 74104). The quality of isolated RNA was critically assessed by Berry Genomics (https://www.berrygenomics.com, Beijing, China). RNA samples for sequencing kept a RIN value greater than 8. Total transcriptome expression analysis was performed. For data analysis, reads mapping was performed with hisat2_2.1.0, featureCounts_2.0.2 was used to count the reads number mapped to each gene, differential gene expression analysis was implemented using DESeq2_1.34.0, DESeq2 was also used to calculate fold change (> 1.5) and *P* value (p value < 0.05 and p.adj < 0.05).

Teratoma formation assay

The mESC cells were digested with 0.05% Trypsin (Thermo Fisher, Cat. no. 15050065), centrifuged and re-suspended cells in 1 mL PBS. Cell density was measured by cell counter, and Matrigel with equal volume was added to make the cell density of 2×10^6 cells/100 μL. Teratoma formation experiments were performed in 8-week-old B-NSG immunodeficient female mice (NOD.CB17-PrkdcscidIl2rgtm1/Bcgen) (Biocytogen, Cat. no. 110586). Cells were injected subcutaneously into the outside of the left hind leg of the recipient mice. Body weight and tumor size were measured

every three days. After 21 days, the mice were sacrificed and tumors were removed for histological analysis.

Grading of immature teratomas

HE-stained sections of teratomas were used for histological grading, we used the modified Thurlbeck-Scully histological grading system for solid ovarian teratomas proposed by Norris et al [24]. The number of neural rosettes was observed in 40X field of view for malignancy grading, grade I has less than 1 neural rosettes in each 40× field of view states as benign teratoma, grade II has 1–3 neural rosettes in each 40× field of view with low malignancy, and more than 3 in each 40× field of view is grade III with malignancy.

Statistical analysis

Data are showed as mean ± SD, differences between groups were determined by unpaired, two-tailed Student's t test. Statistical analysis was performed using GraphPad Prism software 9 (GraphPad Software, La Jolla, CA, USA). $*P<0.05$; $**P<0.01$, $***P<0.001$, P value <0.05 was considered statistically significant.

Results

RetSat localizes onto mitotic chromosomes in stemness positive cells

To investigate the association of RetSat protein and stemness, we first screened its subcellular localization in diverse cell types through immunofluorescence assay using anti-RetSat antibody. We grouped pluripotent stem cell lines such as mouse embryonic stem cells (mESC), mouse induced pluripotent stem cells (miPSC) and human embryonic stem cells (hESC, line H9) as "with stemness" subgroup. In contrast, mouse embryonic fibroblasts (MEF), human somatic fibroblasts (HEL-1) and immortalized HEK293T cells were designated as "without stemness" subgroup (Fig. 1a). Auraro B was used as a mitotic marker. We performed co-immunostaining of anti-RetSat and anti-Auraro B antibodies. Mitotic chromosomes were labeled by DAPI. Strikingly, almost all mitotic cells displayed RetSat location onto chromosomes in "with stemness" subgroup, while this phenomenon was hardly found in "without stemness" subgroup (Fig. 1a-b).

We next sought to validate that RetSat's location on chromosomes is stemness dependent. To this goal, we designed a neuroectodermal and extraembryonic endoderm lineage differentiation assay to remove stemness. mESCs were cultured in feeder-free and LIF-free conditions, plus 0.25 μM retinoic acid (RA) for 48 h and extended culture for two weeks. After differentiation, cell colonies were shifted into fibroblast-like from domal morphologically (Fig. 1c). Loss of stemness was validated through either qPCR or immunoblotting detection of pluripotent markers Oct4 and Sox2 (Fig. 1d-e). We repeated immunostaining assay in both mESC and differentiated cells. After neuronal lineage differentiation, only 5% differentiated cells were detected to have RetSat location of on chromosomes (Fig. 1f-g). In line with neuronal lineage differentiation, when mESCs were cultured in a totally spontaneous differentiation conditions (without LIF factor or RA), the protein level of RetSat was down regulated (Figure S1a-b), and the location of RetSat on chromosomes was also decreased dramatically (Figure S1c).

For further validation, we designed a pluripotency regaining assay (Fig. 1h). We reprogrammed MEF into iPSCs through OSKM transcription factors transduction. After reprogramming, cells were changed into domal colony from flat fibroblasts morphologically (Fig. 1h). Expression of pluripotent markers Oct4 and Sox2 was confirmed by qPCR (Fig. 1i) and immunoblotting (Fig. 1j). The expression of RetSat was increased in iPSCs compared with isogenic MEF counterpart (Fig. 1j). When repeat immunostaining assay, we found that the location rates of RetSat on chromosomes were dramatically increased after pluripotency reprogramming (Fig. 1k-l). Notably, compared with isogenic stemness negative counterparts, both ESCs and iPSCs displayed high expression of RetSat at the transcriptional and protein levels (Fig. 1d-e, i-j), reminding that stemness positive cells may need more RetSat for cellular homeostasis. Taking together, these results indicate that the location of RetSat onto mitotic chromosomes is stemness dependent and dispensable of genetic background.

Loss of RetSat in embryonic stem cells causes chromosome instability

Based on the subcellular location analysis, we next sought to determine the functions of RetSat in pluripotent stem cell chromosomes. To this goal, we derived *RetSat* wild type or knockout embryonic stem cell lines from $RetSat^{WT/WT}$ or $RetSat^{null/null}$ C57/BL6 mice in parallel with the same manipulations (Fig. 2a). Genotyping was validated by semi-quantitative PCR using whole genome DNA (Figure S2a-c). Deletion was confirmed by both qPCR and immunostaining targeting RetSat (Fig. 2c-d). Generally, both $RetSat^{WT/WT}$ or $RetSat^{null/null}$ ESC colonies displayed domal morphology (Fig. 2b). We analyzed pluripotent marker gene expression in $RetSat^{WT/WT}$ or $RetSat^{null/null}$ ESCs. Compared with $RetSat^{WT/WT}$, $RetSat^{null/null}$ ESCs displayed slight down regulation of Oct4, Nanog and Sox2 (Fig. 2c-d). When investigating interphase nuclei morphology by DAPI staining,

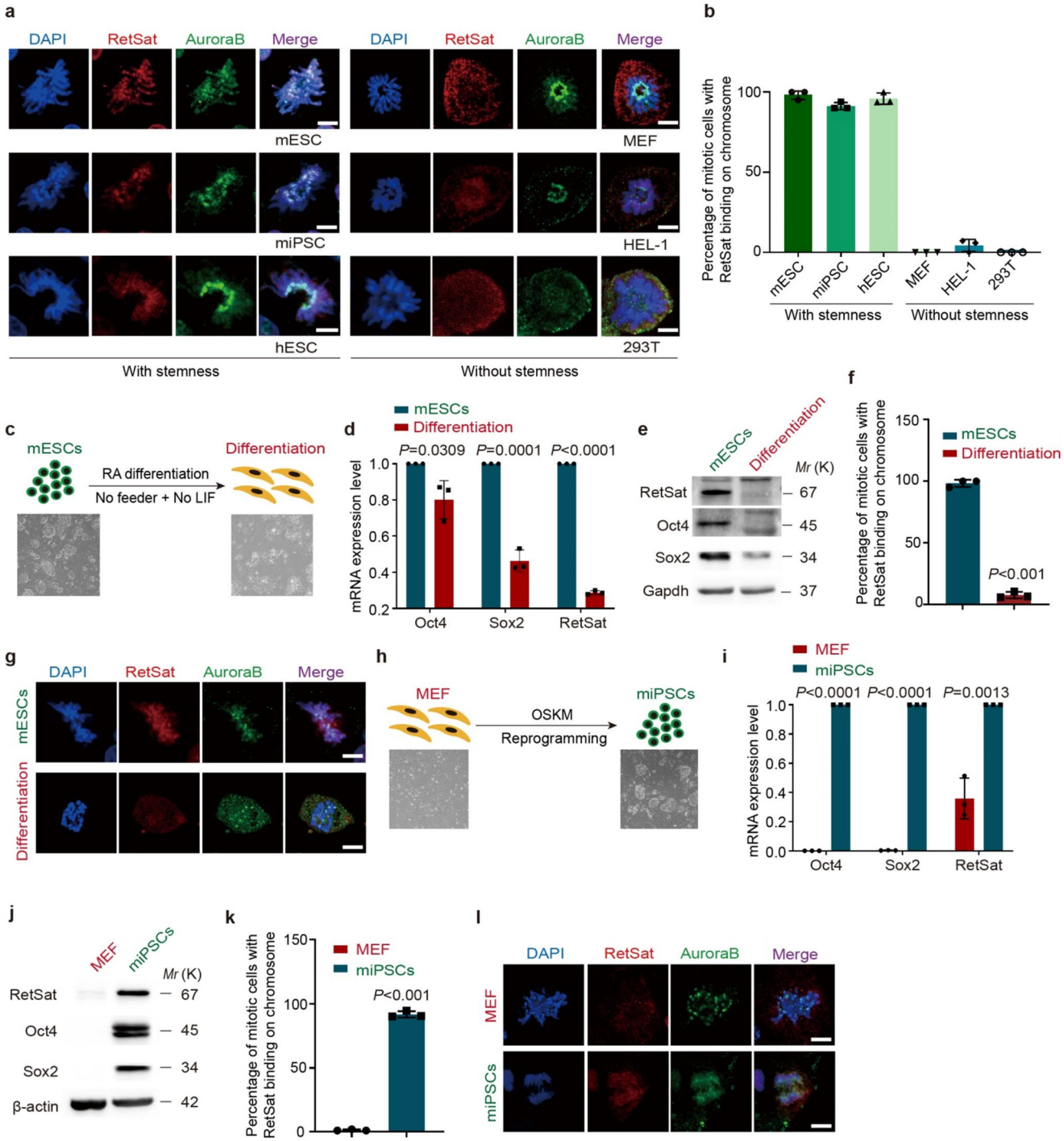

Fig. 1 RatSat localizes onto mitotic chromosomes in pluripotent stem cells. **a-b**: Representative images (**a**) and quantification (**b**) of immunostaining assay using anti-RetSat antibody in designated stemness positive (mESCs, hESCs, miPSCs) and negative (MEF, HEL-1, 293T) cell lines. Aurora B was used as a mitotic marker. Chromosomes were labeled by DAPI. Scale bar represents 5 μm. **c**. Neuronal lineage differentiation of mouse embryonic stem cells using LIF-free, RA-plus procedure. **d-e**: Confirmation of differentiation efficiency using qPCR (**d**) and immunoblotting (**e**). Gapdh was used as an immunoblotting loading control. **f-g**. Percentage (**f**) and representative images (**g**) using anti-RetSat antibody in mitotic mESCs and isogenic differentiation counterparts. $n = 50$ in each group. Scale bar represents 5 μm. **h**. Pluripotency reprogramming of mouse embryonic fibroblasts using Yamanaka factors transduction procedure. **i-j**: Confirmation of pluripotency reprogramming efficiency using qPCR (**i**) and immunoblotting (**j**). β-actin was used as an immunoblotting loading control. **k-l**: Percentage (**k**) and representative images (**l**) using anti-RetSat antibody in mitotic MEFs and isogenic reprogramming counterparts. $n = 50$ in each group. Scale bar represents 5 μm

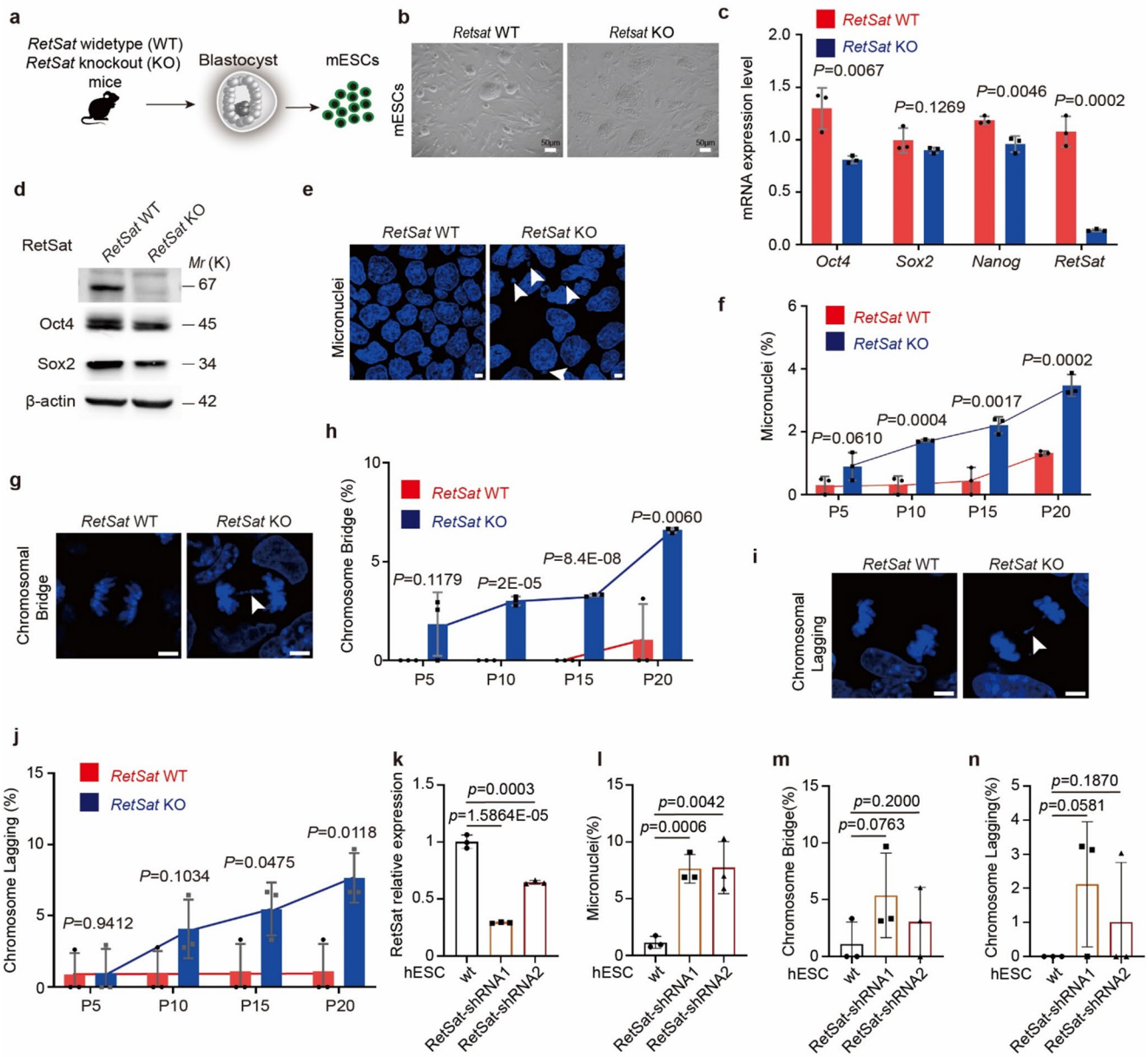

Fig. 2 Loss of RetSat in embryonic stem cells causes chromosome instability. **a**. Derivation of *RetSat* wild type (WT) and knockout (KO) from *RetSat* gene editing mice. **b**. Brightfield morphology of *RetSat* WT and KO mESC colonies. **c-d**: qPCR (**c**) and immunoblotting (**d**) detection of pluripotent markers. Meanwhile, *RetSat* knocking out was confirmed in the same samples. β-actin was used as an immunoblotting loading control. **e-f**: Representative images (**e**) and quantification (**f**) of micronuclei in *RetSat* WT and KO mESCs at consecutive passages. Nuclei were labeled by DAPI. $n = 600$ cells in each group. scale bar represents 5 μm. **g-h**: Representative images (**g**) and quantification (**h**) of mitotic chromosomal bridge in *RetSat* WT and KO mESCs at consecutive passages. Nuclei were labeled by DAPI. $n = 100$ cells in each group. scale bar represents 5 μm. **i-j**: Representative images (**i**) and quantification (**j**) of chromosomal lagging in *RetSat* WT and KO mESCs at consecutive passages. Nuclei were labeled by DAPI. $n = 100$ cells in each group. scale bar represents 5 μm. **k**. qPCR analysis of knocking down *RetSat* in human embryonic stem cells (line H9) using two short hairpin RNAs. **l-n**: Quantification of micronuclei (**l**), chromosomal bridge (**m**) and chromosomal lagging (**n**) occurrence in hESCs with or without *RetSat* knocking down. $n = 100$ cells in each group

we found that $RetSat^{null/null}$ ESCs displayed dramatically high rates of micronuclei (Fig. 2e). We expanded both $RetSat^{WT/WT}$ and $RetSat^{null/null}$ mESCs for twenty passages (three days per passage, totally around sixty days), and calculated micronuclei rates in each five passages. Compared with $RetSat^{WT/WT}$, $RetSat^{null/null}$ ESCs displayed much faster accumulation of micronuclei during the examining time window (Fig. 2f). We also examined chromosomal stability in anaphase in mESC with or without RetSat. We found that $RetSat^{null/null}$ ESCs displayed higher rates of chromosomal

bridge (Fig. 2g-h) and lagging (Fig. 2i-j) compared with *RetSat*$^{WT/WT}$. Similar to micronuclei, the occurrence of both chromosomal bridge and lagging also displayed accumulative effects in the process of continuous expansion. To validate the functional conservation of RetSat, we also knocked down (KD) *RETSAT* gene in human embryonic stem cells (hESCs, line H9) using two short hairpin RNAs targeting different sites (Fig. 2k). After fifteen days consecutive expansion, *RETSAT* -KD hESCs also displayed chromosome instability phenotypes similar to observations in mESCs, with significantly high rate of micronuclei in *RETSAT*-KD groups compared with vector control (Fig. 2l-n).

For further confirmation, we infected *RetSat*$^{null/null}$ ESCs with lentiviral vector expressing mouse *RetSat* CDS region and green fluorescent protein (GFP) tag to construct a RetSat rescued cell line. We isolated GFP positive cells for expansion and validated the rescue effect (Figure S3a-c). RetSat addition rescued micronuclei (Figure S3d), chromosomal bridge (Figure S3e) and lagging (Figure S3f) in *RetSat*$^{null/null}$ ESCs significantly. Notably, compared with *RetSat*$^{WT/WT}$, statistics showed that the chromosome instability in *RetSat*$^{null/null}$ ESCs was rescued partially, but not totally, reminding us that intrinsic changes may occur in the process of cell culture and expansion.

In addition to the comparison under homeostatic culture condition, we also used aphidicolin and reversine to induce genotoxic stress for further validation of RetSat's function [26]. Regarding reversine treatment, we set up three doses (0.5 μM, 1 μM and 2 μM) for 2 h pulse treatment and recovery for 24 h, of which 2 μM reversine treatment caused massive cell death, so we excluded this dose in the following chromosome instability analysis (Figure S4a-c). We also treated cells with 1.25 μM, 2.5 μM or 5 μM aphidicolin for 2 h pulse treatment and recovery for 24 h (Figure S4d-f). *RetSat*$^{null/null}$ ESCs displayed dramatically high rates of chromosome instability compared to wild type counterparts. Especially under 5 μM aphidicolin treatment, the chromosome bridge and lagging rates in *RetSat*$^{null/null}$ ESCs were around two-fold higher than wild type (Figure S4e-f). Together, these results indicate that RetSat is responsible for chromosome stabilization in embryonic stem cells.

RetSat deletion increased ESC carcinogenic risk and impaired embryonic development

To evaluate the influences of *RetSat* deletion on embryonic stem cell homeostasis, we collected *RetSat*$^{WT/WT}$ and *RetSat*$^{null/null}$ mESCs in 20th passage for RNA sequencing (Fig. 3a). Four biological repeats were included in each line. Through differential gene expression (DEG) analysis, we identified 289 upregulated and 173 downregulated DEGs with fold-change values greater than 1.5 (FDR < 0.05) in *RetSat*$^{null/null}$ versus *RetSat*$^{WT/WT}$ mESCs (Fig. 3b, Supplementary Table 1). We performed KEGG (Kyoto Encyclopedia of Genes and Genomes) analysis using these genes (Fig. 3c, Figure S5). Notably, upregulated genes were enriched into many cancer-related pathways such as "breast cancer", "gastric cancer", and "pathways in cancer" (Fig. 3c). Heatmap of 28 cancer-related genes are shown in Fig. 3d.

KEGG analysis revealed that *RetSat*$^{null/null}$ mESC unregulated cancer associated genes, reminding carcinogenic risk in mESC without RetSat. We therefore performed in vivo teratoma formation assay in NOD scid gamma (NSG) mice (Fig. 4a). Five mice were used for each group. *RetSat*$^{WT/WT}$ and *RetSat*$^{null/null}$ mESCs were injected into NSG mice subcutaneously. Teratoma size was monitored every three days. After 21 days post injection, mice were sacrificed to collect tumors for analysis. Compared to *RetSat*$^{WT/WT}$ counterparts, *RetSat*$^{null/null}$ teratoma grew much faster (Fig. 4b-d). Teratoma were cut into slices for H&E staining. Consistent to chromosomal instability phenotypes in in vitro cultured *RetSat*$^{null/null}$ mESCs, we found significantly high level of chromosomal bridge (Fig. 4e-f) and lagging (Fig. 4g-h) in mitotic *RetSat*$^{null/null}$ teratoma cells. *RetSat*$^{null/null}$ teratoma displayed immature status and high malignancy, depending on Thurlbeck-Scully histological grading system (Fig. 4i) [24]. In addition, we checked embryonic development at embryonic day 13.5 with or without RetSat. Compared with *RetSat*$^{WT/WT}$ mouse embryos, around 20% *RetSat*$^{null/null}$ embryos were observed to be stillbirths, showing to be black bruises morphologically (Fig. 4j-k). Together, these results support the notion that *RetSat* is crucial for maintenance of embryonic stem cell identity and embryonic development.

RetSat may stabilize mitotic chromosome condensation in embryonic stem cells

Compared to differentiated counterparts, embryonic stem cells need specific cohesin and condensin regulation networks to balance self-renewal and differentiation elaborately, through which activates pluripotency genes meanwhile represses lineage specification genes [27]. On the other hand, embryonic stem cells grow much faster than differentiated counterparts, relying on effective replication-coupled mechanisms to maintain genome integrity [28]. This indicates embryonic stem cells also require balancing chromosome stability and pluripotency when passing through mitosis repeatedly. Indeed, classical chromosomal structure regulators such as Smc1, Smc3 or even pluripotency factor Nanog have been reported to be functional in genomic stability and stemness maintenance of embryonic stem cells [29, 30]. Currently, it is still quite unclear regarding the triple balancing strategies among chromosome stability, pluripotency and stemness in embryonic stem cells.

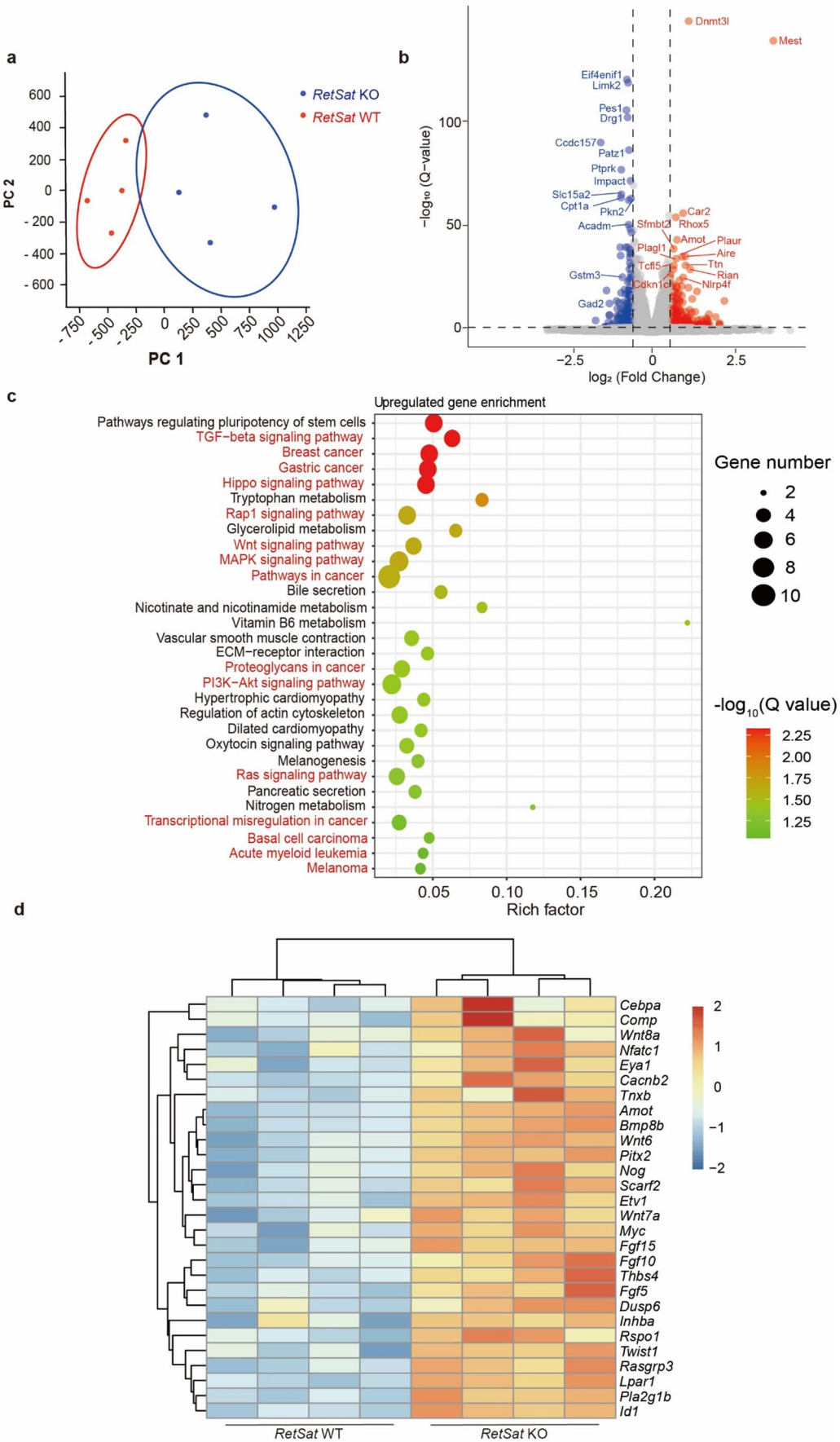
a
RetSat KO
RetSat WT
PC 2
PC 1
b
Dnmt3l
Mest
Eif4enif1
Limk2
Pes1
Drg1
Ccdc157
Patz1
Ptprk
Impact
Slc15a2
Cpt1a
Pkn2
Acadm
Car2
Rhox5
Sfmbt2
Amot
Plaur
Plagl1
Aire
Tcfl5
Ttn
Rian
Gstm3
Cdkn1c
Nlrp4f
Gad2
−log10 (Q−value)
log2 (Fold Change)
c
Upregulated gene enrichment
Pathways regulating pluripotency of stem cells
TGF−beta signaling pathway
Breast cancer
Gastric cancer
Hippo signaling pathway
Tryptophan metabolism
Rap1 signaling pathway
Glycerolipid metabolism
Wnt signaling pathway
MAPK signaling pathway
Pathways in cancer
Bile secretion
Nicotinate and nicotinamide metabolism
Vitamin B6 metabolism
Vascular smooth muscle contraction
ECM−receptor interaction
Proteoglycans in cancer
PI3K−Akt signaling pathway
Hypertrophic cardiomyopathy
Regulation of actin cytoskeleton
Dilated cardiomyopathy
Oxytocin signaling pathway
Melanogenesis
Ras signaling pathway
Pancreatic secretion
Nitrogen metabolism
Transcriptional misregulation in cancer
Basal cell carcinoma
Acute myeloid leukemia
Melanoma
Rich factor
Gene number
-log10(Q value)
d
Cebpa
Comp
Wnt8a
Nfatc1
Eya1
Cacnb2
Tnxb
Amot
Bmp8b
Wnt6
Pitx2
Nog
Scarf2
Etv1
Wnt7a
Myc
Fgf15
Fgf10
Thbs4
Fgf5
Dusp6
Inhba
Rspo1
Twist1
Rasgrp3
Lpar1
Pla2g1b
Id1
RetSat WT
RetSat KO

Fig. 3 Transcriptome comparison between *RetSat* WT and KO mESCs. **a**. Bulk RNA sequencing and Principal Component Analysis (PCA) of *RetSat* WT and KO mESCs. **b**. Volcano plot of different expression genes (DEGs) in *RetSat* KO mESCs versus WT. **c**. Kyoto Encyclopedia of Genes and Genomes analysis (KEGG) of upregulated DEGs in RetSat KO mESCs versus WT. **d**. Heatmap of carcinogenesis associated genes in *RetSat* KO mESCs versus WT

So we next sought to check whether RetSat has an connection to known chromosome structure regulatory network. To this goal, we collected mitotic mESCs and performed immunoprecipitation combined with mass spectrometry analysis targeting endogenous RetSat. We set up both anti-IgG and *RetSat*-KO samples as negative controls (Fig. 5a). Through exclusion of non-specific binding peptides, 43 proteins were identified to be potential interacting factors of RetSat (Fig. 5b, Supplementary Table 2). In this list, we focused on Nudcd2, a cohesin component for further validation [31]. The interaction of RetSat and Nudcd2 was validated using co-immunoprecipitation combined with immunoblotting assay (Fig. 5c). Besides, RetSat also displayed interaction with Smc1a, but not Smc3 (Fig. 5c). Notably, both whole-cell levels and chromosome binding dosages of Nudcd2 and Smc1a were compromised in *RetSat*-KO mESCs compared with wild type control (Fig. 5d). Although RetSat did not interact with Smc3, RetSat deletion caused chromosomal

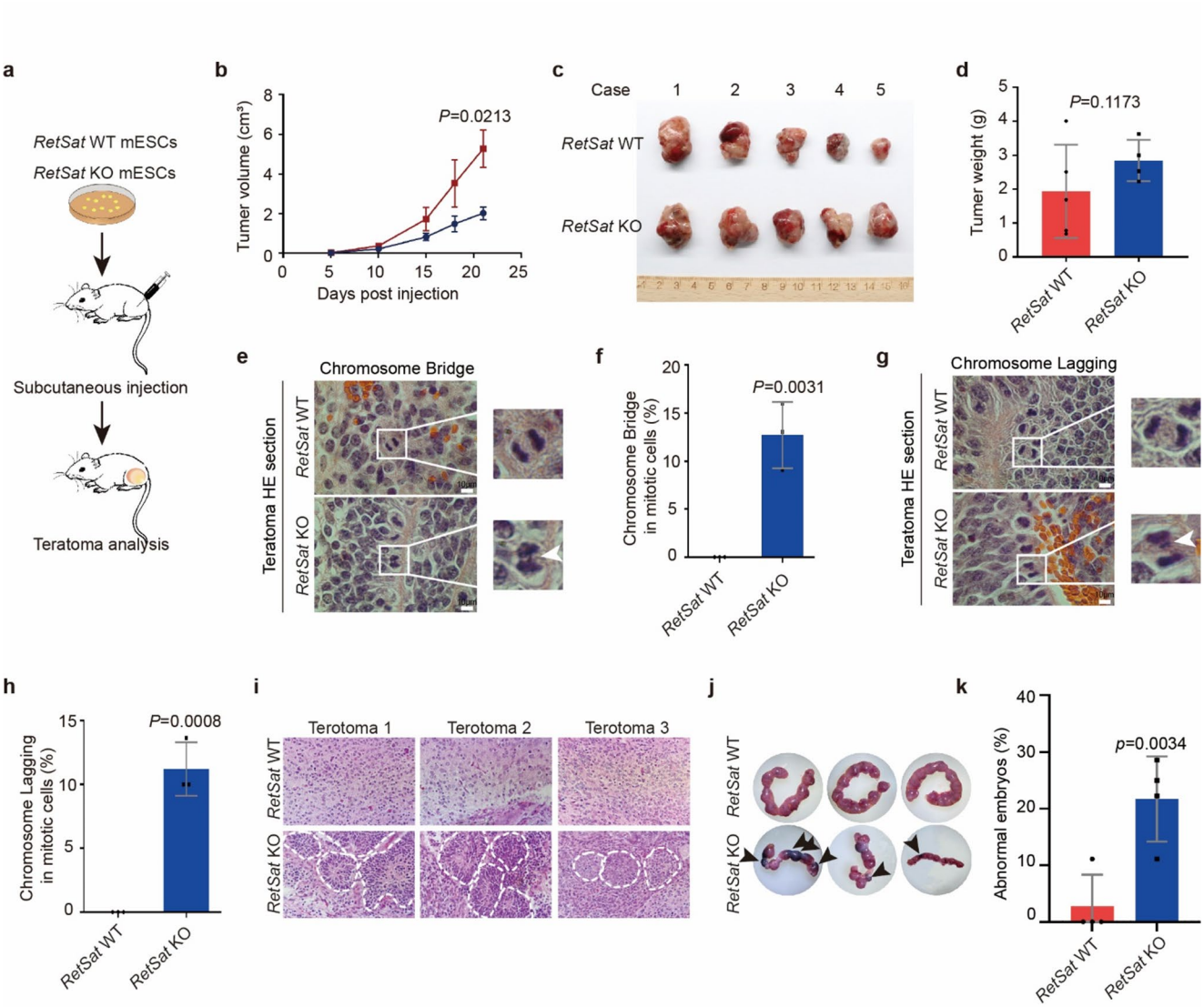

Fig. 4 RetSat deletion caused high carcinogenic risk in mESCs. **a**. Illustration of teratoma formation assay. Five NOD-SCID mice were used in each group. **b-c**. Tumor volume monitoring (**b**) and tumor pictures (**c**) derived from *RetSat* WT or KO mESCs, respectively. **d**. Weight comparison between *RetSat* WT and KO teratoma. **e-f**. Representative images (**e**) and quantification (**f**) of chromosomal bridge in *RetSat* WT or KO teratoma. $n = 60$ mitotic cells were calculated in each group. Scale bar = 10 μm. **g-h**. Representative images (**e**) and quantification (**f**) of chromosomal lagging in *RetSat* WT or KO teratoma. $n = 60$ mitotic cells were calculated in each group. Scale bar = 10 μm. **i**. H&E staining of teratoma slices from *RetSat* WT or KO mESCs. **j-k**. Representative images (**j**) and quantification (**k**) of fetal development at embryonic day 13.5. $n = 9$ in each group

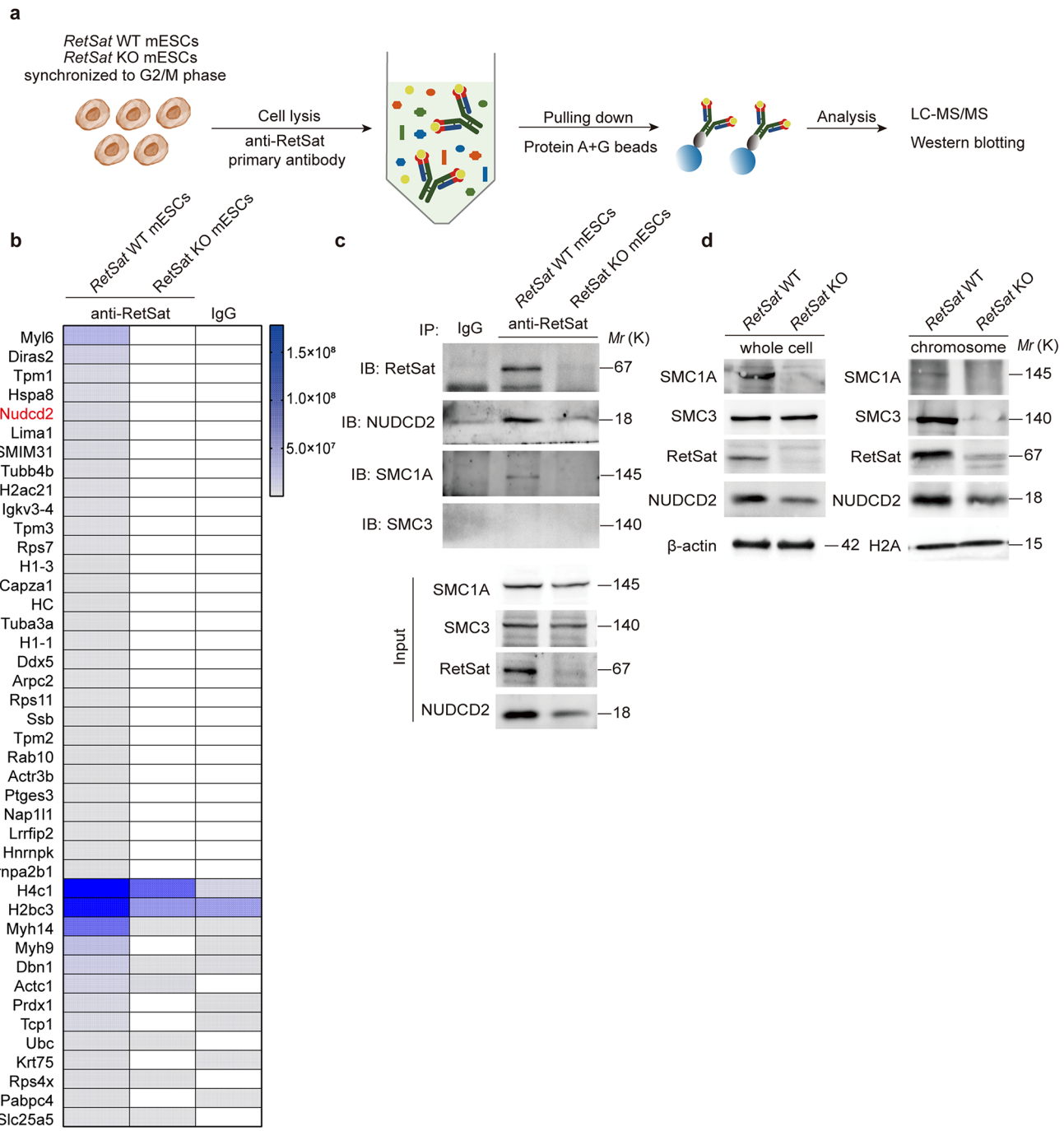

Fig. 5 RetSat interacts with chromosome condensation components Nudcd2. **a**. Illustration of immunoprecipitation combined with LC-MS/MS in mitotic mESCs using anti-RetSat antibody. Isotypical IgG and RetSat KO mitotic cells were set up as negative controls. **b**. Heatmap of potential RetSat interactome based on LC-MS/MS identification results. **c**. Co-immunoprecipitation (co-IP) in lysis from mitotic RetSat WT mESCs. Isotypic IgG and RetSat KO mitotic cells were set up as negative controls. **d**. Immunoblotting detection of Smc1a, Smc3 and Nudcd2 in whole-cell lysis from *RetSat* WT or KO mESCs, respectively. b actin was used as a loading control. **e**. Immunoblotting detection of Smc1a, Smc3 and Nudcd2 in chromosomal lysis from *RetSat* WT or KO mESCs, respectively. H2A was used as a loading control

mis-loading of Smc3 (Fig. 5e). Together, these results support the notion that RetSat is a key regulator for chromosome stability in embryonic stem cells.

Discussion

In this study, we report the pivotal role of *RetSat*, a pluripotent stem cells highly expressed gene in chromosomal stability maintenance. Through techniques such as immunofluorescence staining, transcriptomic analysis, and xenograft experiments in mice, we confirmed that RetSat primarily governs the binding abundance of cohesin/condensin complex components Nudcd2, Smc1a, and Smc3 on chromosomes. In comparison to differentiated cells, the expression level of RetSat is significantly elevated in pluripotent stem cells. This conclusion has been substantiated through both forward spontaneous differentiation experiments and reverse reprogramming experiments. Indeed, it has been unveiled that pluripotent stem cells use some specific regulators to maintain genomic stability, such as coding genes *Filia* [7], *Floped* [9], as well as non-coding LncRNA *Lnc956* [10], *Discn* [13]. Here we showed that RetSat also displayed characters similar to these regulators. Future studies need to be addressed regarding the upstream regulation (transcriptional factors or functional elements) of RetSat, as well as its potential interaction to these well-defined pluripotency-specific regulators. Deletion of RetSat results in a significant decrease in the expression levels of classical pluripotency factors such as Oct4, Nanog, and Sox2. This suggests a potential association between RetSat and the classical pluripotency regulatory network. Combined with the reported evidence in 4C viewpoints between RetSat and Nanog [23], there may be unique upstream regulatory patterns of RetSat in pluripotent stem cells.

Some questions need to be answered in the future. First, as a highly expressed gene in pluripotent stem cells, the mechanism by which RetSat itself is recruited to chromosomes requires further investigation. Second, existing studies have revealed high expression levels of RetSat in cells of tissues such as adipose, predominantly localized in cellular compartments like the endoplasmic reticulum within the cytoplasm [32]. This implies that RetSat may exert diverse functions based on tissue specificity, cell specificity, or cell cycle specificity. Based on our mass spectrometry analysis results, RetSat may interact with other proteins that not confirmed in this study. How does RetSat function in diverse biological contexts is still unclear. Third, the occurrence of aneuploidy in early embryonic cells across different species is common [33]. For example, approximately 70% of human early embryonic cells exhibit aneuploidy [1], while the proportion of aneuploid cells in early mouse embryos is only about 5% [34]. In this study, we confirmed the functional conservation of RetSat protein in chromosomal stability in both mouse and human pluripotent stem cells, underscores the significance of RetSat's function. We also found that RetSat deletion impaired late-stage embryonic development (Fig. 4j). The detailed function and mechanism of RetSat in late-stage embryonic development is still unknown. Forth, the prospective applications of pluripotent stem cells in translational medicine are highly anticipated. We found that RetSat deletion increased carcinogenic risk of embryonic stem cells. This reminded the potential value of RetSat as an effective biomarker for assessing the quality of pluripotent stem cells.

Conclusion

Chromosomal stability is critical for not only normal embryonic development, but also for safety control of in vitro cultured pluripotent stem cells (PSC) in translational application. Matching with PSCs' characters such as high-proliferation and pluripotency, PSCs may need unique factors to achieve their high demand in chromosomal stability maintenance. In this study, we identified PSC high-expressed RetSat protein as a key stabilizer of chromosome condensation in pluripotent stem cells. Understanding the functions and mechanism of RetSat in chromosomal stabilization will promote the early-stage embryonic development research, meanwhile be valuable of PSC quality control in translational medicine.

Supplementary Information The online version contains supplementary material available at https://doi.org/10.1007/s00018-024-05413-x.

Acknowledgements The authors would like to thank animal facility at Kunming Institute of Zoology, Chinese Academy of Sciences for assistance in animal assays. This work was supported by the National Natural Science Foundation of China (32388102, 31930011 to P.S.), the foundation of Yunnan Revitalization Talent Support Program Science & Technology Champion Project (202305AB350002 to P.S.), the National Key Research & Developmental Program of China (2021YFA0805701 to B.Z.), the Applied Basic Research. Programs of Science and Technology Commission Foundation of Yunnan Province (202201AS070044 to B.Z.), Yunnan Province (202305AH340006 to B.Z.) and Kunming Science and Technology Bureau (2022SCP007 to B.Z.).

Author contributions W.C. and X.Y., carried out most of the experimental works, collected and analyzed the data. G.L. conducted the RNA-seq analysis, drew the heatmap of cancer related genes, bubble chart of KEGG pathways and volcano plot of DEGs. X.L. conducted the knock-down of *RetSat* in hESCs and assessed chromosome instability. P.S. and B.Z. designed and supervised experiments, and wrote the manuscript.

Data availability RNA sequencing and mass spectrometry data is

available at Genome Sequence Archive (GSA) (https://ngdc.cncb.ac.cn/gsa/), Project accession: PRJCA018513. The data sets used and/or analyzed during the current study are available from the leading corresponding author (ship@mail.kiz.ac.cn) on reasonable request.

Declarations

Ethics approval and consent to participate The "Comparison of teratoma formation efficacy of RetSat wild type and knockout mouse embryonic stem cells in NOD-SCID mice" was established following the guidelines of Institutional Animal Care and Use Committee of Kunming Institute of Zoology, Chinese Academy of Sciences. All experiments conducted on animals were approved by the Institutional Animal Care and Use Committee of Kunming Institute of Zoology, Chinese Academy of Sciences (Approval No: SMKX-20200710-37). The approval date was July 10, 2020.

Consent for publication Not Applicable.

Competing interests The authors declare that they have no competing interests.

References

1. Mertzanidou A et al (2013) Microarray analysis reveals abnormal chromosomal complements in over 70% of 14 normally developing human embryos. Hum Reprod 28(1):256–264
2. Meriano J et al (2004) Binucleated and micronucleated blastomeres in embryos derived from human assisted reproduction cycles. Reprod Biomed Online 9(5):511–520
3. Takahashi K, Yamanaka S (2006) Induction of pluripotent stem cells from mouse embryonic and adult fibroblast cultures by defined factors. Cell 126(4):663–676
4. Wang J, Sun S, Deng H (2023) Chemical reprogramming for cell fate manipulation: methods, applications, and perspectives. Cell Stem Cell 30(9):1130–1147
5. Andrews PW et al (2022) The consequences of recurrent genetic and epigenetic variants in human pluripotent stem cells. Cell Stem Cell 29(12):1624–1636
6. Choi EH et al (2022) Meiosis-specific cohesin complexes display essential and distinct roles in mitotic embryonic stem cell chromosomes. Genome Biol 23(1):70
7. Zhao B et al (2015) Filia is an ESC-Specific Regulator of DNA damage response and safeguards genomic Stability. Cell Stem Cell 16(6):684–698
8. Ma H et al (2023) Lnc956 regulates mouse embryonic stem cell differentiation in response to DNA damage in a p53-independent pathway. Sci Adv 9(3):eade9742
9. Zhao B et al (2018) Mouse embryonic stem cells have increased capacity for replication fork restart driven by the specific Filia-Floped protein complex. Cell Res 28(1):69–89
10. Zhang W et al (2023) Lnc956-TRIM28-HSP90B1 complex on replication forks promotes CMG helicase retention to ensure stem cell genomic stability and embryogenesis. Sci Adv 9(4):eadf6277
11. Zalzman M et al (2010) Zscan4 regulates telomere elongation and genomic stability in ES cells. Nature 464(7290):858–863
12. Le R et al (2021) Dcaf11 activates Zscan4-mediated alternative telomere lengthening in early embryos and embryonic stem cells. Cell Stem Cell 28(4):732–747e9
13. Wang L et al (2021) A novel lncRNA Discn fine-tunes replication protein A (RPA) availability to promote genomic stability. Nat Commun, 12(1)
14. Palmerola KL et al (2022) Replication stress impairs chromosome segregation and preimplantation development in human embryos. Cell 185(16):2988–3007e20
15. Moise AR et al (2004) Identification of all-trans-retinol: All-trans-13,14-dihydroretinol saturase. J Biol Chem 279(48):50230–50242
16. Heidenreich S et al (2017) Retinol saturase coordinates liver metabolism by regulating ChREBP activity. Nat Commun 8(1):384
17. Sun Y et al (2008) Identification and characterization of a novel mouse peroxisome proliferator-activated receptor alpha-regulated and starvation-induced gene, Ppsig. Int J Biochem Cell Biol 40(9):1775–1791
18. Schupp M et al (2009) Retinol saturase promotes adipogenesis and is downregulated in obesity. Proc Natl Acad Sci USA 106(4):1105–1110
19. Shin DJ et al (2012) Genome-wide analysis of FoxO1 binding in hepatic chromatin: potential involvement of FoxO1 in linking retinoid signaling to hepatic gluconeogenesis. Nucleic Acids Res 40(22):11499–11509
20. Xu D et al (2021) A single mutation underlying phenotypic convergence for hypoxia adaptation on the Qinghai-Tibetan Plateau. Cell Res 31(9):1032–1035
21. Tu Q et al (2022) RETSAT associates with DDX39B to promote fork restarting and resistance to gemcitabine based chemotherapy in pancreatic ductal adenocarcinoma. J Exp Clin Cancer Res 41(1):274
22. Nagaoka-Yasuda R et al (2007) An RNAi-based genetic screen for oxidative stress resistance reveals retinol saturase as a mediator of stress resistance. Free Radic Biol Med 43(5):781–788
23. de Wit E et al (2013) The pluripotent genome in three dimensions is shaped around pluripotency factors. Nature 501(7466):227–
24. Lo Curto M et al (2007) Mature and immature teratomas: results of the first paediatric Italian study. Pediatr Surg Int 23(4):315–322
25. Tu Q et al (2022) RETSAT associates with DDX39B to promote fork restarting and resistance to gemcitabine based chemotherapy in pancreatic ductal adenocarcinoma. J Experimental Clin Cancer Res, 41(1)
26. Santaguida S et al (2017) Chromosome mis-segregation generates cell-cycle-arrested cells with Complex Karyotypes that are eliminated by the Immune System. Dev Cell 41(6):638–651e5
27. Cuadrado A et al (2019) Specific contributions of Cohesin-SA1 and Cohesin-SA2 to TADs and polycomb domains in embryonic stem cells. Cell Rep 27(12):3500–3510e4
28. Ahuja AK et al (2016) A short G1 phase imposes constitutive replication stress and fork remodelling in mouse embryonic stem cells. Nat Commun 7:10660
29. Lin T et al (2005) 53 induces differentiation of mouse embryonic stem cells by suppressing nanog expression. Nat Cell Biol 7(2):165–171

30. Yoon S et al (2023) Alpha-kleisin subunit of cohesin preserves the genome integrity of embryonic stem cells. BMB Rep 56(2):108–113
31. Yang YH et al (2019) NudCL2 is an Hsp90 cochaperone to regulate sister chromatid cohesion by stabilizing cohesin subunits. Cell Mol Life Sci 76(2):381–395
32. Weber P et al (2020) Retinol Saturase: more than the name suggests. Trends Pharmacol Sci 41(6):418–427
33. Cavazza T et al (2021) Parental genome unification is highly error-prone in mammalian embryos. Cell 184(11):2860–
34. Pauerova T et al (2020) Aneuploidy during the onset of mouse embryo development. Reproduction 160(5):773–782